Transverse momentum resummation at small *x* for the Fermilab Tevatron and CERN LHC

Stefan Berge,[1,*] Pavel M. Nadolsky,[2,†] Fredrick I. Olness,[1,‡] and C.-P. Yuan[3,§]

[1]*Department of Physics, Southern Methodist University, Dallas, Texas 75275-0175, USA*

[2]*High Energy Physics Division, Argonne National Laboratory, Argonne, Illinois 60439-4815, USA*

[3]*Michigan State University, Department of Physics and Astronomy, East Lansing, Michigan 48824-1116, USA*

(Received 19 November 2004; published 24 August 2005)

Analysis of semi-inclusive hadroproduction in deep inelastic scattering suggests broadening of transverse momentum distributions at x below a few 10^{-3}, which can be modeled in the Collins-Soper-Sterman formalism by a modification of impact-parameter-dependent parton densities. We discuss the consequences of such a modification for the production of electroweak bosons at hadron-hadron colliders. If substantial small-x broadening is observed in forward Z^0 boson production in the Tevatron Run-2, it will strongly affect predicted q_T distributions for $W^\pm$, Z^0, and Higgs boson production at the Large Hadron Collider.

I. INTRODUCTION

Moderately heavy particles with masses about 100 GeV can be copiously produced in hadron collisions at TeV energies. Production and observation of such particles is accompanied by intense hadronic activity, which affects overall rates and differential cross sections. Radiation of several hadrons of relatively low energy may produce a strong recoil effect on the heavy particle. Calculations in perturbative quantum chromodynamics (PQCD) may have to be reorganized to resum large logarithms associated with multiple hadronic radiation.

Electroweak symmetry breaking in the standard model introduces vector bosons $W^\pm$ and Z^0 with masses of about 80 and 91 GeV, and a scalar Higgs boson H^0 with a likely mass below 250 GeV, as suggested by global fits of electroweak data. Supersymmetric extensions of the standard model require existence of several types of scalar bosons, with the lightest naturally having a mass below about 140 GeV in the minimal supersymmetric standard model [1]. Identification of heavy bosons relies on understanding of transverse momentum distributions for heavy bosons and their decay products, as well as for background processes. Short-lived bosons are commonly detected by observing their decay into a pair of color-neutral particles with large transverse momenta (of order of a half of the boson's mass) in the laboratory reference frame. Furthermore, the mass M_V of the heavy boson (e.g., W boson) can be determined from the transverse momentum distribution of the decay products.

When the boson's transverse momentum q_T is much smaller than the boson's virtuality Q, the calculation of the transverse momentum distribution must evaluate an all-order sum of large logarithms $\ln^n(q_T/Q)$. The resummation of logarithms at small q_T can be realized using one of several available methods; see [2–7] for some recent references. As stated by Collins, Soper, and Sterman (CSS) in Ref. [8], at moderate energies all large logarithms are generated by a product of a soft (Sudakov) exponential and special parton distribution functions in the impact parameter (b) space. The b-space resummed form factor can be evaluated in PQCD at large Q ($Q^2 \gg \Lambda_{QCD}^2$) and small b ($b^2 \ll \Lambda_{QCD}^{-2}$). Its calculation is possible due to the collinear factorization of hadronic cross sections, valid when Q is not small compared to the total energy $\sqrt{S}$ of the hadronic collision. The CSS approach describes well the available q_T data from fixed-target Drell-Yan experiments and Z boson production at the Tevatron [9].

In this paper,[1] we discuss possible deviations from this established picture that may occur in the new range of energies accessible to the Large Hadron Collider (LHC). As we move from the 1.96 TeV $p\bar{p}$ collider Tevatron to the 14 TeV pp collider LHC, the typical fraction of the collision energy going into production of moderately heavy bosons decreases below 1%, leading to several new effects. Transverse momentum distributions of W and Z bosons can be altered at small momentum fractions x by increased contributions from qg and gg hard scattering, which tends to produce electroweak bosons with larger transverse momenta as compared to the dominant process of $q\bar{q}$ scattering. One also expects enhancement of the logarithms $\ln(1/x)$ in the matrix elements of order α_s^2 and beyond, the effect not completely accounted for in the conventional q_T resummation. Such logarithms may be enhanced by a larger QCD coupling strength α_s at q_T less than a few GeV, even when they are negligible in inclusive cross

---

*E-mail: berge@mail.physics.smu.edu

†E-mail: nadolsky@hep.anl.gov

‡E-mail: olness@smu.edu

§E-mail: yuan@pa.msu.edu

[1]Our results were partly presented in Ref. [10] as a contribution to the 3d Les Houches workshop "Physics at TeV colliders" [11].

sections depending on one hard scale $Q \gg 1$ GeV. Finally, complex nonperturbative dynamics contributing at $b \gtrsim 1$ GeV^{-1} may also depend on x. At present, the magnitude of the x-dependent corrections to W, Z, and Higgs boson production at the LHC energy is largely unknown, in part because no experimental data on q_T distributions is available yet in Drell-Yan-like processes at x of a few 10^{-3} or less.

Resummation of q_T logarithms at $q_T/Q \to 0$ and $x \gg 0$ is realized in the Dokshitzer-Gribov-Lipatov-Altarelli-Parisi (DGLAP) picture of hadronic scattering [12–15], which assumes that the dominant parton emissions are strongly ordered in transverse momenta. At asymptotically high collision energies ($x \sim Q/\sqrt{S} \to 0$ with q_T/Q fixed), the collinear DGLAP factorization is superseded by the off-shell factorization in the Balitsky-Fadin-Kuraev-Lipatov (BFKL) framework [16–18], which sums up leading logarithms of $1/x$, while including q_T logarithms at a finite order of α_s only. When neither DGLAP nor BFKL dynamics dominates (for instance, when both x and q_T are small), methods for simultaneous summation of q_T and $1/x$ logarithms (e.g., the Ciafaloni-Catani-Fiorani-Marchesini equation [19–22]) may be needed. Together with the increased magnitude of qg and gg scattering, reduced convergence of the perturbation series in the DGLAP framework may signal transition to the small-x dynamical regime at the existing colliders.

Some of the transition phenomena may be already observed in part of phase space at Hadron-Electron Ring Accelerator (HERA) at DESY. The analog of the Drell-Yan process in lepton-nucleon deep inelastic scattering (DIS) is semi-inclusive production of hadronic final states, $e + p \xrightarrow{\gamma^*} e + \text{hadron(s)} + X$. The CSS resummation formalism can be applied to semi-inclusive deep inelastic scattering (SIDIS) to describe the dependence on the Lorentz-invariant transverse momentum q_T [23,24]. Refs. [25,26] have compared predictions of q_T resummation to the data for the transverse energy flow in the current fragmentation region [27,28]. The experimentally observed q_T distribution at x below 10^{-2} becomes wider as x decreases. This ''broadening'' of q_T distributions was modeled by including an extra x-dependent term in the resummed form factor. To describe the data, the extra term must grow quickly as $x \to 0$. It provides a phenomenological parametrization for all substantial factors responsible for x dependence beyond that included in the $\mathcal{O}(\alpha_s)$ resummed q_T cross section. For example, large corrections from hard scattering of order $\mathcal{O}(\alpha_s^2)$ substantially modify the SIDIS cross section at large transverse momenta [29–32], and such corrections are also likely important at small q_T (not discussed in the published studies). Apart from the hard-scattering contributions, the dynamics of collinear radiation may change at moderately small x ($x < 10^{-2}$) and small energy scales ($1/b < 1 - 2$ GeV) as a result of

preasymptotic suppression of gluon splittings by BFKL logarithms [33]. Both enhancement of perturbative scattering at larger q_T and preasymptotic BFKL suppression of collinear radiation at smaller q_T would result in broader q_T distributions.

While a systematic framework describing all x-dependent effects is yet to be developed, some predictions can be made by exploiting universality of soft and collinear radiative corrections, which dominate the SIDIS energy flow data at $q_T < 2 - 3$ GeV. For this reason, we employ the phenomenological parametrization for the small-q_T cross section found in SIDIS to predict the x dependence of q_T distributions at $x \lesssim 10^{-2}$ at hadron-hadron colliders. The proposed new form of the Drell-Yan resummed form factor at $x \lesssim 10^{-2}$ is given by

$$\widetilde{W}(b, Q) = \widetilde{W}_{BLNY}(b, Q) e^{-\rho(x_A)b^2 - \rho(x_B)b^2}, \qquad (1)$$

where $\widetilde{W}_{BLNY}(b, Q)$ is the resummed form factor found in the global fit [9] to the Drell-Yan data at larger x, and the exponential $e^{-\rho(x_A)b^2 - \rho(x_B)b^2}$ parametrizes the small-x broadening.

New phenomena at small momentum fractions may have consequences for precision measurements and searches for new physics. Modifications in the transverse momentum distributions for W and Z bosons will affect the measurements of the W boson mass and width, as well as the W and Z boson background in the search for new gauge bosons, supersymmetry, particle compositeness, extra spatial dimensions, etc. At the LHC, the q_T broadening may affect detection of the Higgs bosons by altering q_T distributions of Higgs bosons and the relevant QCD background.

We examine possible small-x effects in W, Z, and Higgs boson production at the Tevatron and LHC. Sizable q_T broadening may occur at both colliders. The validity of our model can be tested in the immediate future by the analysis of forward-rapidity q_T distributions in the Tevatron Run-2. An observation of signs of q_T broadening at the Tevatron will suggest a large magnitude of this effect at the LHC.

In Section II, we propose a relationship between the SIDIS and Drell-Yan q_T distributions based on factorization properties of the CSS resummed cross section. To describe the enhanced x-dependent contributions, we include in the resummed form factor an additional phenomenological term determined from the SIDIS data. In Section III, we predict within this model the q_T distributions in production of W and Z bosons in the forward region at the Tevatron and the central region at the LHC. We also explore implications for light Higgs boson production via gluon-gluon fusion at the LHC. The appendix reviews the rapidity coverage at the existing hadron colliders.

II. RELATIONSHIP BETWEEN THE RESUMMED CROSS SECTIONS IN DRELL-YAN AND SEMI-INCLUSIVE DIS PROCESSES

A. Resummed form factor in electroweak boson production

We start by discussing production of the electroweak bosons at moderate collision energies $\sqrt{S}$, when the ratio $Q/\sqrt{S}$ is large, but not very close to unity. At such energies, the logarithms $\ln(x)$ or $\ln(1-x)$ of the partonic momentum fractions x are of a moderate magnitude in most of the events. This situation is typical for the production of Drell-Yan lepton pairs in fixed-target experiments and W or Z bosons at the Tevatron.

At small transverse momenta q_T, the differential cross section takes the form [8]

$$\frac{d\sigma}{dQ^2 dy dq_T^2} = \int_0^\infty \frac{bdb}{2\pi} J_0(q_T b)\widetilde{W}(b, Q, x_A, x_B)$$
$$+ Y(q_T, Q, x_A, x_B), \qquad (2)$$

where $y = (1/2)\ln[(E + p_z)/(E - p_z)]$ is the rapidity of the vector boson, $x_{A,B} \equiv Qe^{\pm y}/\sqrt{S}$ are the Born-level partonic momentum fractions, and $J_0(q_T b)$ is the Bessel function. The integral is the Fourier-Bessel transform of a form factor $\widetilde{W}(b, Q, x_A, x_B)$, given in impact parameter (b) space. It contains an all-order sum of the logarithms $\alpha_s^n \ln^m(q_T^2/Q^2)$, which dominates in the small-q_T region. $Y(q_T, Q, x_A, x_B)$ is the regular part, defined as the difference of the fixed-order cross section and expansion of the Fourier-Bessel integral to the same order of α_s. It is numerically small at $q_T \to 0$.

$\widetilde{W}(b, Q, x_A, x_B)$ can be expressed as a product of Born-level prefactors $\sigma_{ab}^{(0)}$, a Sudakov exponent $e^{-S(b,Q)}$, and b-space parton distributions $\overline{\mathcal{P}}_a^{(T)}(x, b)$:

$$\widetilde{W}(b, Q, x_A, x_B) = \frac{\pi}{S}\sum_{a,b}\sigma_{ab}^{(0)}e^{-S(b,Q)}\overline{\mathcal{P}}_a^{(T)}(x_A, b)\overline{\mathcal{P}}_b^{(T)}(x_B, b).$$
$$(3)$$

This form will be referred to as "the CSS representation." It has been stated as a factorization theorem in Ref. [8] and recently proved in Ref. [34].[2] The summation in Eq. (3) is over the relevant parton flavors a and b. In the approximation of a vanishing width of the boson, the nonzero Born-level prefactors are given by

$$\sigma_{i\bar{j}}^{(0)} = \frac{\pi}{3}\sqrt{2}M_W^2 G_F |V_{ij}|^2 \delta(Q^2 - M_W^2) \qquad (4)$$

in W boson production for $i = u, d, \dots, \bar{j} = \bar{u}, \bar{d}, \dots$;

$$\sigma_{i\bar{i}}^{(0)} = \frac{\pi}{12}\sqrt{2}M_Z^2 G_F((1 - 4|e_i|\sin^2\theta_w)^2 + 1)\delta(Q^2 - M_Z^2)$$
$$(5)$$

in Z boson production for $i = u, d, \dots$; and

$$\sigma_{gg}^{(0)} = \frac{\alpha_s^2 Q^2}{576\pi}\sqrt{2}G_F \delta(Q^2 - M_H^2) \qquad (6)$$

in Higgs boson production. Here M_W, M_Z, and M_H are the masses of the W, Z, and Higgs bosons, G_F is the Fermi constant, $\theta_w = \sin^{-1}(1 - M_W^2/M_Z^2)$ is the weak mixing angle, V_{ij} is the Cabibbo-Kobayshi-Maskawa matrix, and $e_i = 2/3$ or $-1/3$ are the fractional quark charges for up- or down-type quarks. The prefactor (6) for Higgs boson production is derived by using the effective ggH vertex in the approximation of infinitely heavy top quarks [35–38]. This approximation works well for the Higgs bosons that are lighter than the top quark.

The Sudakov term $S(b, Q)$ is an integral of the functions $\mathcal{A}(\alpha_s(\bar{\mu}))$ and $\mathcal{B}(\alpha_s(\bar{\mu}))$, which can be calculated in PQCD when b is small ($b^2 \ll \Lambda_{QCD}^{-2}$):

$$S(b, Q) = \int_{b_0^2/b^2}^{Q^2}\frac{d\bar{\mu}^2}{\bar{\mu}^2}\left[\mathcal{A}(\alpha_s(\bar{\mu}))\ln\frac{Q^2}{\bar{\mu}^2} + \mathcal{B}(\alpha_s(\bar{\mu}))\right].$$
$$(7)$$

$b_0 \equiv 2e^{-\gamma_E}$ is a constant parameter involving the Euler constant, $\gamma_E = 0.577\dots$ Approximation of $S(b, Q)$ at a finite order of α_s yields "the perturbative Sudakov factor" $S_P(b, Q)$. The perturbative coefficients $\mathcal{A}^{(i)}$ and $\mathcal{B}^{(i)}$ for the functions $\mathcal{A}(\alpha_s(\bar{\mu}))$ and $\mathcal{B}(\alpha_s(\bar{\mu}))$ up to the next-to-next-to-leading order are published in Refs. [8,39,40] for the Drell-Yan process, and Refs. [41–45] for Higgs boson production.[3]

The form factor (3) depends on the light-cone momentum fractions x_A and x_B through the functions $\overline{\mathcal{P}}_a^{(T)}(x, b)$. In the CSS representation, we distinguish between the functions $\overline{\mathcal{P}}_a^{(T)}(x, b)$ and $\overline{\mathcal{P}}_a^{(S)}(x, b)$ appearing in reactions with timelike (T) and spacelike (S) electroweak bosons. The relationship between $\overline{\mathcal{P}}_a^{(T)}(x, b)$ (relevant to the Drell-Yan process) and $\overline{\mathcal{P}}_a^{(S)}(x, b)$ (relevant to SIDIS) is discussed later in this section. Expansion of $\overline{\mathcal{P}}_a^{(T)}(x, b)$ in leading powers of b at $b \to 0$ gives [46]

$$\overline{\mathcal{P}}_a^{(T)}(x, b) = \sum_c \int_x^1 \frac{d\xi}{\xi} C_{a/c}^{\mathrm{in}(T)}\left(\xi, b, \alpha_s\left(\frac{b_0}{b}\right)\right)f_c\left(\frac{x}{\xi}, \frac{b_0}{b}\right) + \dots$$
$$\equiv [C_{a/c}^{\mathrm{in}(T)} \otimes f_c](x, b) + \dots \qquad (8)$$

Here $C_{a/c}^{\mathrm{in}(T)}(x, b, \alpha_s(b_0/b))$ are the Wilson coefficient functions for incoming ("in") partons, and $f_c(x, b_0/b)$ are the conventional parton distributions (integrated over the parton's transverse momentum $\mathbf{k}_T$). The ellipsis denotes the

---

[2]The factorization for the resummed form factors in the Drell-Yan and SIDIS processes has been also demonstrated recently within the framework based on gauge-invariant b-dependent parton distributions [6,7].

[3]Equations in this paper correspond to the "canonical" choice [8] of the momentum scales.

terms that are suppressed by positive powers of b. The renormalization and factorization scales on the right-hand side of Eq. (8) are equal to b_0/b. Whenever the series in powers of $\alpha_s(b_0/b)$ and b in Eq. (8) converge, $\overline{\mathcal{P}}_a^{(T)}(x, b)$ can be approximated by neglecting the positive powers of b, evaluating $C_{a/c}^{\text{in}(T)}$ at a finite order of α_s, and using a parametrization for $f_c(x, \mu)$ from a phenomenological global fit. Estimates for $C_{a/c}^{\text{in}(T)}$ of order $\mathcal{O}(\alpha_s)$ can be found in Refs. [8,42,43].

Contributions from nonperturbative impact parameters ($b \gtrsim 1 \text{ GeV}^{-1}$) are suppressed at $Q \rightarrow \infty$ by the shape of $\widetilde{W}(b, Q, x_A, x_B)$ and oscillations of $J_0(q_T b)$. Nonetheless, mild sensitivity to the large-b behavior remains in W and Z boson production when q_T is of order a few GeV. The factorization of $\widetilde{W}(b, Q, x_A, x_B)$ predicts universality of the nonperturbative terms within classes of similar processes, such as production of Drell-Yan pairs, W, and Z bosons. While the nonperturbative terms cannot be calculated yet from the first principles, they can be introduced in the calculation by using one of the available models. The present Drell-Yan and Z boson data at x above a few 10^{-2} is consistent with universality, as it was demonstrated recently [9] within the "b_*" model [8,47] for the nonperturbative terms. The "b_*" model parametrizes the resummed form factor as

$$\widetilde{W}(b, Q, x_A, x_B) = \widetilde{W}^{pert}(b_*, Q, x_A, x_B)e^{-S_{NP}(b,Q;b_*)}, \quad (9)$$

where

$$\widetilde{W}^{\,\text{pert}}(b_*, Q, x_A, x_B) \equiv \frac{\pi}{S} \sum_{a,b,c,d} \sigma_{ab}^{(0)}[C_{a/c}^{\text{in}(T)} \otimes f_c](x_A, b_*)$$
$$\times [C_{b/d}^{\text{in}(T)} \otimes f_d)](x_B, b_*)e^{-S_P(b_*,Q)} \quad (10)$$

is the perturbative approximation for $\widetilde{W}(b, Q, x_A, x_B)$, evaluated as a function of $b_* \equiv b(1 + b^2/b_{max}^2)^{-1/2}$ for $b_{max} \sim 1 \text{ GeV}^{-1}$. The nonperturbative Sudakov function,

$$S_{NP}(b, Q; b_*) \equiv -\ln\left[\frac{\widetilde{W}(b, Q, x_A, x_B)}{\widetilde{W}^{\text{pert}}(b_*, Q, x_A, x_B)}\right], \quad (11)$$

is determined from the experimental data. If the flavor dependence of large-b contributions is neglected (a reasonable first approximation in reactions dominated by the scattering of u and d quarks), $S_{NP}(b, Q; b_*)$ is straightforwardly related to the true Sudakov factor $S(b, Q)$ and b-dependent parton distributions $\overline{\mathcal{P}}_a^{(T)}(x_A, b)$ in Eq. (3):

$$S_{NP}(b, Q; b_*) \approx S(b, Q) - S_P(b_*, Q) - \ln\left(\frac{\overline{\mathcal{P}}_a^{(T)}(x_A, b)}{\overline{\mathcal{P}}_a^{(T)}(x_A, b_*)}\right)$$
$$- \ln\left(\frac{\overline{\mathcal{P}}_b^{(T)}(x_B, b)}{\overline{\mathcal{P}}_b^{(T)}(x_B, b_*)}\right). \quad (12)$$

This representation realizes the generic form for $S_{NP}(b, Q; b_*)$ found in Ref. [8],

$$S_{NP}(b, Q; b_*) = g_S(b, \ln Q; b_*) + g_a(b, x_A; b_*)$$
$$+ g_b(b, x_B; b_*),$$

where g_S, g_a, and g_b are some functions of the shown arguments. Several analyses have been carried out in the past in order to constrain $S_{NP}(b, Q; b_*)$ from the Drell-Yan data [48–52]. In the present work, we use the BLNY parametrization S_{NP}^{BLNY} [9], given by

$$S_{NP}^{BLNY}(b, Q; b_*) = \left[0.21 + 0.68 \ln\left(\frac{Q}{3.2 \text{ GeV}}\right)\right.$$
$$\left. - 0.126 \ln(100 x_A x_B)\right]b^2 \quad (13)$$

for $b_{max} = 0.5 \text{ GeV}^{-1}$. This choice of parameters yields good agreement with the Drell-Yan data and is convenient for comparison with the q_T fit in SIDIS, which was also performed for $b_{max} = 0.5 \text{ GeV}^{-1}$. Alternative forms for the parametrization of $\widetilde{W}(b, Q, x_A, x_B)$ at large b have been also considered [3,5,53]. Studies [54,55] of the general structure of the large-b contributions with the methods of infrared renormalon analysis have demonstrated, in particular, that the leading power-suppressed contribution is quadratic in b (Gaussian), i.e., that $S_{NP} \sim b^2$, as in Eq. (13).

Since $x_A x_B = Q^2/S$, $S_{NP}^{BLNY}(b, Q; b_*)$ is independent of the boson's rapidity. It will be used in Section III to predict the W and Z boson resummed cross sections in the case when all rapidity dependence is contributed by $[C_{a/c}^{\text{in}(T)} \otimes f_c](x, b_0/b)$. By comparing Eqs. (12) and (13), we find that the logarithmic combination of $\overline{\mathcal{P}}_a^{(T)}(x, b)$,

$$\ln\left(\frac{\overline{\mathcal{P}}_a^{(T)}(x, b)}{\overline{\mathcal{P}}_a^{(T)}(x, b_*)}\right) \approx \ln\left(\frac{\overline{\mathcal{P}}_a^{(T)}(x, b)}{[C_{a/c}^{\text{in}(T)} \otimes f_c](x, \frac{b_0}{b_*})}\right) \equiv c^{(T)}(x, b; b_*),$$
$$(14)$$

is a slowly varying function of x (denoted by $c^{(T)}(x, b; b_*)$). Therefore,

$$\overline{\mathcal{P}}_a^{(T)}(x, b) \approx [C_{a/c}^{\text{in}(T)} \otimes f_c](x, b_*)e^{c^{(T)}(x,b;b_*)}, \quad (15)$$

when x is larger than a few percent.

The nonperturbative function $S_{NP}(b, Q; b_*)$ may take a different form in gluon-dominated Higgs boson production. Fortunately, the sensitivity to $S_{NP}(b, Q; b_*)$ is suppressed in gluon-initiated channels at the LHC by a larger color factor associated with the perturbative leading-logarithm contributions. In Section III C 2, we quantitatively estimate the effect of the uncertainty in $S_{NP}(b, Q; b_*)$ on the Higgs boson cross section.

B. Resummed form factor at small x

As $x \to 0$, the approximation (15) for $\overline{\mathcal{P}}_a^{(T)}(x, b)$ may be altered because of the reduced convergence of the perturbation series at intermediate and large impact parameters. The factorized expression (3) for $\widetilde{W}(b, Q, x_A, x_B)$ is derived from the requirements of renormalization- and gauge-group invariance, and does not rely on the perturbative convergence for the individual components, including $\overline{\mathcal{P}}_a^{(T)}(x, b)$. Similar factorization holds for the resummed form factor in semi-inclusive deep inelastic scattering (SIDIS), $e + A \xrightarrow{\gamma^*} e + B + X$ [6,23–25], where A and B are the initial- and final-state hadrons, respectively. SIDIS probes the x-dependence of the *spacelike* distributions $\overline{\mathcal{P}}_j^{(S)}(x, b)$ for *quark* flavors ($j = u, d, \dots$), which differ from the timelike quark distributions $\overline{\mathcal{P}}_j^{(T)}(x, b)$ by a factor $r(b)$:

$$\overline{\mathcal{P}}_j^{(T)}(x, b) = r(b)\overline{\mathcal{P}}_j^{(S)}(x, b). \qquad (16)$$

This relationship is derived in Section II D, which also shows that $r(b)$ is independent of x.

The experimentally observed hadronic energy flow in SIDIS [27,28] is compatible with the following form of $\overline{\mathcal{P}}_j^{(S)}(x, b)$ [25,26] at $10^{-4} \lesssim x \lesssim 1$:

$10^{-4} \lesssim x \lesssim 1$:

$$\overline{\mathcal{P}}_j^{(S)}(x, b) \approx [C_{j/a}^{\text{in}(S)} \otimes f_a](x, b_*)e^{-0.013b^2/x + c^{(S)}(x, b; b_*)}, \quad (17)$$

with

$$C_{j/a}^{\text{in}(S)}(x, b_*) = \frac{1}{r(b_*)}C_{j/a}^{\text{in}(T)}(x, b_*). \qquad (18)$$

The exponential $\exp(-0.013b^2/x)$ results in the additional x-dependent broadening of the q_T distributions. The power of the exponential, $0.013b^2/x$, is small at $x \gg 10^{-2}$ and rapidly grows at $10^{-4} < x < 10^{-2}$. The SIDIS fit does not constrain $\overline{\mathcal{P}}_j^{(S)}(x, b)$ at $x < 10^{-4}$. The $1/x$ growth of the exponential power may be modified at very small x by the turn-on of other scattering mechanisms, notably BFKL resummation and saturation. The remaining terms (collectively denoted as $c^{(S)}(x, b; b_*)$) do not depend strongly on x and can be numerically important only at large x and b. The behavior of $\overline{\mathcal{P}}_j^{(S)}(x, b)$ in the transition region $x \sim 10^{-2}$ and precise form of $c^{(S)}(x, b; b_*)$ are not well determined by the SIDIS fit because of the limited accuracy of the data.

According to Eq. (16), the broadening exponential must also be present in the timelike distributions $\overline{\mathcal{P}}_j^{(T)}(x, b)$ and dominate at moderately small x:

$10^{-4} < x < 10^{-2}$:

$$\overline{\mathcal{P}}_j^{(T)}(x, b) \approx [C_{j/a}^{\text{in}(T)} \otimes f_a](x, b_*)e^{-0.013b^2/x + c^{(T)}(x, b; b_*)}. \quad (19)$$

The functions $c^{(T)}(x, b; b_*)$ and $c^{(S)}(x, b; b_*)$ are in principle related by

$$c^{(T)}(x, b; b_*) = c^{(S)}(x, b; b_*) + \ln\left[\frac{r(b)}{r(b_*)}\right]. \qquad (20)$$

We find that the large-x form (9) of the resummed form factor is quantitatively known from the fits to the Drell-Yan and Tevatron Run-1 Z boson data, while the leading behavior at $x < 10^{-2}$ can be inferred from SIDIS. What is not precisely known is the behavior of $\overline{\mathcal{P}}_j^{(T)}(x, b)$ in the transition region around $x \sim 10^{-2}$. To estimate the possible impact on the Tevatron and LHC observables, we interpolate $\overline{\mathcal{P}}_j^{(T)}(x, b)$ between the large-x parametrization (15) and small-x parametrization (19) by using a smooth trial function $\rho(x)$:

$10^{-4} \lesssim x < 1$:

$$\overline{\mathcal{P}}_j^{(T)}(x, b) \approx [C_{j/a}^{\text{in}(T)} \otimes f_a](x, b_*)e^{-\rho(x)b^2 + c^{(T)}(x, b; b_*)}. \qquad (21)$$

We choose $\rho(x)$ as

$$\rho(x) = c_0\left(\sqrt{\frac{1}{x^2} + \frac{1}{x_0^2}} - \frac{1}{x_0}\right), \qquad (22)$$

where c_0 controls the magnitude of the broadening for a given x, and x_0 is a characteristic value of x below which $\rho(x)$ becomes non-negligible. In the limits $x \gg x_0$ and $x \ll x_0$, Eq. (21) reduces to the large-x form (15) and small-x form (19), respectively. As a result of the new form for $\overline{\mathcal{P}}_j^{(T)}(x, b)$, the BLNY representation (9) is multiplied by $e^{-\rho(x_A)b^2 - \rho(x_B)b^2}$:

$$\widetilde{W}(b, Q, x_A, x_B) = \frac{\pi}{S}\sum_{a,b,c,d}\sigma_{ab}^{(0)}[C_{a/c}^{\text{in}(T)} \otimes f_c]\left(x_A, b_*\right)$$
$$\times [C_{b/d}^{\text{in}(T)} \otimes f_d]\left(x_B, b_*\right)$$
$$\times e^{-S_P(b_*, Q) - S_{NP}^{BLNY}(b, Q; b_*)}e^{-b^2\rho(x_A) - b^2\rho(x_B)}.$$
$$(23)$$

Equation (9) is restored from Eq. (23) when both x_A and x_B are much larger than x_0. The Gaussian exponential $e^{-\rho(x)b^2}$ approximately preserves the integral of the q_T distribution, and the observables inclusive in q_T remain essentially unaffected. To reproduce the leading small-x behavior in Eq. (19), our quantitative estimates for W and Z boson cross sections in Section III are made for $c_0 = 0.013$ and $x_0 = 0.005$. We will also consider variations around these values to examine sensitivity of the Tevatron W and Z production to various broadening scenarios. The cross sections for Higgs boson production are computed for two values of c_0, 0.013 and 0.026, in order to evaluate the uncertainty due to the unknown small-x form

of the gluon distribution $\overline{\mathcal{P}}_g^{(T)}(x, b)$ (not constrained by the SIDIS data).

C. Resummed z flow

In the remainder of this section, we review the resummation in SIDIS $e(k) + A(p_A) \xrightarrow{\gamma^*(q)} e(k') + B(p_B) + X$ and its relationship to the resummation in the Drell-Yan process. The x dependence of the distribution $\overline{\mathcal{P}}_a^{(S)}(x, b)$ can be determined from the data on the hadronic z-flow Σ_z, defined by [56–58]

$$\Sigma_z \equiv \sum_B \int_{z_{\min}}^1 z\sigma(e + A \rightarrow e + B + X)dz. \tag{24}$$

The z-flow is obtained from the product of the cross section and final-state light-cone variable $z = (p_B \cdot p_A)/(q \cdot p_A)$ by integrating over z and summing over all final-state hadrons B. It is related to the pseudorapidity (η) distribution of the transverse energy flow $\langle E_T \rangle$ in the center-of-mass frame (c.m.) of the virtual photon and initial-state hadron A (with γ^* moving in the $+z$ direction):

$$q_T^2 \frac{d\Sigma_z}{dxdQ^2dq_T} \equiv \frac{d\langle E_T \rangle}{dxdQ^2d\eta}, \tag{25}$$

where $Q^2 = -q^2 > 0$, and $x \equiv Q^2/(2p_A \cdot q)$. The Lorentz-invariant transverse momentum q_T is a function of η, $q_T = Q(x^{-1} - 1)^{1/2}e^{-\eta}$ [25]. The resummation applies in the limit $q_T \rightarrow 0$, which corresponds to the current fragmentation region in the photon-hadron c.m. frame ($\eta \rightarrow +\infty$). In this limit, the enhanced soft and collinear logarithms in the theory prediction must be summed to all orders.

Similarly to the Drell-Yan case of Eq. (2), the resummed z-flow is given by a combination of the Fourier-Bessel transform integral and finite term Y_z:

$$\frac{d\Sigma_z}{dxdQ^2dq_T^2} = \int_0^\infty \frac{bdb}{2\pi} J_0(q_Tb)\tilde{W}_z(b, Q, x)$$
$$+ Y_z(q_T, Q, x). \tag{26}$$

Under HERA conditions, the finite piece $Y_z(q_T, Q, x)$ is small at $q_T < 2 - 3$ GeV. The analysis of the SIDIS z-flow at such q_T probes universal soft and collinear radiation described by the resummed Fourier-Bessel integral. The form factor $\tilde{W}_z(b, Q, x)$ is structurally close to the resummed form factor (3) in the Drell-Yan process:

$$\tilde{W}_z(b, Q, x) = \frac{\pi}{S_{eA}} \sum_{j=u,\bar{u},d,\bar{d},...} \sigma_j^{(0)} e^{-S(b,Q)} C_z^{\text{out}}(b)\overline{\mathcal{P}}_j^{(S)}(x, b), \tag{27}$$

where $S_{eA} \equiv (k + p_A)^2$,

$$\sigma_j^{(0)} \equiv \frac{8\pi\alpha_{EM}^2}{S_{eA}x^2}\left(1 - \frac{2}{y_{DIS}} + \frac{2}{y_{DIS}^2}\right)e_j^2, \tag{28}$$

and $y_{DIS} \equiv Q^2/(xS_{eA})$. The structure of the Sudakov exponent $S(b, Q)$ is displayed in Eq. (7). The spacelike distributions $\overline{\mathcal{P}}_j^{(S)}(x, b)$ factorize at small b as

$$\overline{\mathcal{P}}_j^{(S)}(x, b)|_{b^2 \ll \Lambda_{QCD}^{-2}} = [C_{j/a}^{\text{in}(S)} \otimes f_a](x, b), \tag{29}$$

where $C_{j/a}^{\text{in}(S)}(x, b, \alpha_s(b_0/b))$ are the spacelike Wilson coefficient functions for incoming partons. $C_z^{\text{out}}(b)$ is a residual from the summation over the hadronic final states:

$$C_z^{\text{out}}(b) = 1 + \frac{\alpha_s(b_0/b)}{\pi}C_F\left(-1 - \frac{\pi^2}{3}\right) + ... \tag{30}$$

The right-hand side of Eq. (27) depends on x via $\overline{P}_j^{(S)}(x, b)$. Nonperturbative contributions to the z-flow can be parametrized using the b_* prescription:

$$\tilde{W}_z(b, Q, x) = \frac{\pi}{S_{eA}} \sum_{j=u,\bar{u},d,\bar{d},...} \sigma_j^{(0)} C_z^{\text{out}}(b_*)$$
$$\times [C_{j/a}^{\text{in}} \otimes f_a](x, b_*)e^{-S_P(b_*,Q)-S_{NP}^z(b,Q,x;b_*)}, \tag{31}$$

where $S_{NP}^z(b, Q, x; b_*)$ was found from an $\mathcal{O}(\alpha_s)$ fit [26] to the data [27,28] at $8 \times 10^{-5} \leq \langle x \rangle \leq 0.11$ and $10 \leq \langle Q^2 \rangle \leq 2200$ GeV^2. The leading small-x behavior of $S_{NP}^z(b, Q, x; b_*)$ is consistent with inverse power dependence:

$$S_{NP}^z(b, Q, x; b_*) \approx \frac{c_0b^2}{x^p} + ... \tag{32}$$

The best fit in Ref. [26] quotes $c_0 = 0.013$ and $p = 1$. The x-dependence shown in Eq. (32) describes, in particular, the data at $q_T < 2 - 3$ GeV, where the uncertainties due to the matching (switching) between the W and Y terms are small. By comparing two forms (27) and (31) for $\tilde{W}_z(b, Q, x)$, we find that the leading small-x term is a part of $\overline{\mathcal{P}}_j^{(S)}(x, b)$, in agreement with Eq. (17):

$$\overline{\mathcal{P}}_j^{(S)}(x, b) \approx [C_{j/a}^{\text{in}(S)} \otimes f_a](x, b_*)e^{-(0.013b^2/x)+c^{(S)}(x,b;b_*)}. \tag{33}$$

Theoretical uncertainties in the parametrization of $\overline{\mathcal{P}}_j^{(S)}(x, b)$ due to final-state fragmentation, matching, and higher-order corrections to the Y-term are reduced by our choice of the experimental observable (z-flow) and kinematical region (q_T less than a few GeV). The exponential factor $e^{-0.013b^2/x}$ parametrizes the full contribution of higher-order radiative corrections of diverse wavelengths to $\overline{\mathcal{P}}_j^{(S)}(x, b)$. It indicates that the SIDIS q_T distributions tend to become wider at smaller x, and it attributes the observed broadening to scattering at $b^2 \gtrsim 0.013/x$. At $x = 10^{-2}$ (10^{-4}), this inequality translates into $b_0/b < b_0(x/0.013)^{-1/2} \approx 1.3$ (13) GeV, i.e., only scattering at low and intermediate energy scales is affected.

Several intense mechanisms beyond $\mathcal{O}(\alpha_s)$ may turn on at such small x and $1/b$ and cause the broadening. The rate may be increased at larger q_T ($1/b > 1 - 2$ GeV) by enhanced contributions from qg and gg hard scattering, as it happens in $\mathcal{O}(\alpha_s^2)$ SIDIS cross sections at $p_T = zq_T \sim Q$ [29–32]. The rate may be reduced at smaller q_T ($1/b < 1 - 2$ GeV) in the probed range of x because of the suppression of collinear splittings of gluons by the logarithms $\ln(1/x)$ at higher orders of α_s [33]. In addition to these leading-power (logarithmic in b) contributions, the x dependence may also arise from the unknown nonperturbative terms in $\overline{\mathcal{P}}_j^{(S)}(x, b)$ proportional to the positive powers of b. In the absence of a systematic computation of all such effects in the resummation formalism, the phenomenological broadening exponential serves as an approximate model of their total impact in the limited range $10^{-4} < x < 10^{-2}$ covered by the H1 data. The form of $\overline{\mathcal{P}}_j^{(S)}(x, b)$ is unknown at x outside of the H1 data range, so that the parametrization (33) may not be extrapolated to x below 10^{-4}.

D. Relationship between resummation in DY and SIDIS

The remaining step in the derivation of Eq. (23) is the relationship (16) between the timelike distributions $\overline{\mathcal{P}}_j^{(T)}(x, b)$ and spacelike distributions $\overline{\mathcal{P}}_j^{(S)}(x, b)$. This relationship follows from an elementary representation for spacelike ($I = S$) and timelike ($I = T$) distributions $\overline{\mathcal{P}}_j^{(I)}(x, b)$ [47]:

$$\overline{\mathcal{P}}_j^{(I)}(x, b) = |\mathcal{H}_j^{(I)}(b_0/b)|\tilde{U}(b_0/b)^{1/2}\hat{\mathcal{P}}_j(x, b). \quad (34)$$

The function $\mathcal{H}_j^{(I)}(b_0/b) = 1 + (\alpha_s(b_0/b)/\pi)\mathcal{H}_j^{(1,I)} + \dots$ is composed of highly virtual corrections to the hard-scattering vertex. The function $\tilde{U}(b_0/b)^{1/2}$ collects the soft subgraphs that are attached by gluon propagators to $\mathcal{H}_j^{(I)}(b_0/b)$. It is the same for $I = S$ and $I = T$. $\hat{\mathcal{P}}_j(x, b)$ is related to the $(n - 2)$-dimensional Fourier-Bessel transform of the unintegrated ($\mathbf{k}_T$-dependent) parton distribution function $\mathcal{P}_j(x, \mathbf{k}_T, \zeta)$,

$$\hat{\mathcal{P}}_j(x, b) = \lim_{\zeta \to \infty}\left\{e^{S'(b,\zeta)}\int d^{n-2}\mathbf{k}_T e^{i\mathbf{k}_T \cdot \mathbf{b}}\mathcal{P}_j(x, \mathbf{k}_T, \zeta)\right\}. \quad (35)$$

$\mathcal{P}_j(x, \mathbf{k}_T, \zeta)$ is given in terms of the quark field ψ_j by

$$\begin{aligned}\mathcal{P}_j(x, \mathbf{k}_T, \zeta) = \sum_{\text{spin}}\sum_{\text{color}}\int\frac{dy^- d^2\mathbf{y}_T}{(2\pi)^3} \\ \times e^{-ixp^+y^- + i\mathbf{k}_T \cdot \mathbf{y}_T}\langle p|\bar{\psi}_j(0^+, y^-, \mathbf{y}_T) \\ \times \frac{\gamma^+}{2}\psi_j(0)|p\rangle,\end{aligned} \quad (36)$$

in a gauge $n \cdot \mathcal{A} = 0$ with $n^2 < 0$. It depends on the gauge through the parameter $\zeta \equiv (p \cdot n)/|n^2|$, where p^μ is the momentum of the parent hadron. $\hat{\mathcal{P}}_j(x, b)$ is obtained from $\mathcal{P}_j(x, \mathbf{k}_T, \zeta)$ by taking the limit $\zeta \to \infty$. The partial Sudakov factor $S'(b, \zeta)$ in Eq. (35) was derived in Ref. [59]. The function $\hat{\mathcal{P}}_j(x, b)$ is the same in SIDIS and Drell-Yan processes [34].

Among the three terms on the right-hand side of Eq. (34), only the hard vertex $\mathcal{H}_j^{(I)}$ depends on the sign of the boson's virtuality. The functions $\mathcal{H}_j^{(T)}$ and $\mathcal{H}_j^{(S)}$ are given by the same Feynman graphs in the different crossed channels, i.e., for bosons of timelike virtualities in the Drell-Yan case and spacelike virtualities in the SIDIS case. Therefore,

$$\overline{\mathcal{P}}_j^{(T)}(x, b) = \frac{|\mathcal{H}_j^{(T)}(b_0/b)|}{|\mathcal{H}_j^{(S)}(b_0/b)|}\overline{\mathcal{P}}_j^{(S)}(x, b) = r(b)\overline{\mathcal{P}}_j^{(S)}(x, b),$$
$$(37)$$

where

$$r(b) \equiv \frac{|\mathcal{H}_j^{(T)}(b_0/b)|}{|\mathcal{H}_j^{(S)}(b_0/b)|} = 1 + \alpha_s\left(\frac{b_0}{b}\right)\pi\frac{C_F}{4} + \dots \quad (38)$$

A similar consideration for $b = b_*$ proves the relationship (18) between $C_{j/a}^{\text{in}(S)}(x, b_*)$ and $C_{j/a}^{\text{in}(T)}(x, b_*)$, as well as the relationship (20) between $c^{(T)}(x, b; b_*)$ and $c^{(S)}(x, b; b_*)$.

According to Eq. (34), the dependence of the parton distributions $\overline{\mathcal{P}}_j^{(T)}(x, b)$ and $\overline{\mathcal{P}}_j^{(S)}(x, b)$ on x is determined by the same function $\hat{\mathcal{P}}_j(x, b)$. More generally, the x dependence of the distributions $\overline{\mathcal{P}}_a^{(I)}(x, b)$ ($a = g, u, d, \dots$) is determined by the type of the parent hadron and parton flavor, but not by the type of the produced electroweak final state. For example, the x dependence of $\overline{\mathcal{P}}_a^{(I)}(x, b)$ is expected to be the same in the Drell-Yan process, $\gamma\gamma$ production via $q\bar{q}$ annihilation, and SIDIS; or in Higgs boson production and $\gamma\gamma$ production via gg fusion. This happens because all dependence of $\overline{\mathcal{P}}_a^{(I)}(x, b)$ on the hard-scattering process is determined by the hard vertex function $\mathcal{H}_a^{(I)}(b_0/b)$ [45], which does not contain x. $\overline{\mathcal{P}}_a(x, b)$ are automatically process-independent in the representations for $\tilde{W}(b, Q, x_A, x_B)$ that always separate $\mathcal{H}_a^{(I)}$ from $\overline{\mathcal{P}}_a(x, b)$ [45,47,59]. The best-fit phenomenological functions $S_{NP}^{BLNY}(b, Q; b_*)$ and $S_{NP}^z(b, Q; b_*)$ were obtained in the CSS representation. For this reason, we will use this representation in the numerical analysis despite the additional complexities in the factorization relations.

III. NUMERICAL RESULTS

A. Overview

In this section, we compare the resummed cross sections (23) with the additional broadening term [$\rho(x) \neq 0$] to the resummed cross sections without such a term [$\rho(x) = 0$]. We consider the decay modes $W^{\pm} \rightarrow e\nu$, $Z^0 \rightarrow e\bar{e}$, and $H^0 \rightarrow \gamma\gamma$ and discuss the impact of the experimental acceptance cuts imposed on the decay particles. The resummation calculations that include the decay of the vector and scalar bosons were described in Refs. [60,61], respectively. The perturbative Sudakov factor was included up to $\mathcal{O}(\alpha_s^2)$, and the functions $[C^{\text{in}(T)} \otimes f]$ up to $\mathcal{O}(\alpha_s)$. The numerical calculation was performed using the programs Legacy and ResBos [9,60], and with the CTEQ6M parton distribution functions [62].

For the chosen parameters, the small-x broadening occurs when one or both longitudinal momentum fractions $x_{A,B} \approx M_V e^{\pm y}/\sqrt{S}$ are of order, or less than, $x_0 = 0.005$. The accessible ranges of x_A, x_B, and y at the Tevatron and LHC are displayed in Fig. 1. Lower values of x_A can be reached at the price of pushing x_B closer to unity, and vice versa. The number of events affected by the broadening can be determined from the rapidity distributions $d\sigma/dy$ in Fig. 2.[4] In all scattering processes, most of the events occur at relatively small $|y|$. The rate in the forward regions is suppressed by the decreasing parton densities at $x \rightarrow 1$. The broadening can be detected at all boson rapidities if $\sqrt{S} \gtrsim M_V/x_0$, or at forward rapidities $|y| \gtrsim \ln[M_V/(\sqrt{S}x_0)]$, if the cross section is large enough to measure the q_T distribution at such $|y|$. The heavy bosons are identified in the experiment by observation of secondary particles from their decay. The magnitude of the broadening depends on the procedure applied to select the decay leptons or photons. The estimates for W bosons are modified by the integration over the unobserved rapidity of the neutrino, which mixes contributions from different ranges of y. The impact of the boson's decay will be addressed quantitatively in the next subsections.

In the Tevatron Run-2 ($\sqrt{S} = 1.96$ TeV), the W and Z bosons are predominantly produced at $x_A \sim x_B \sim M_V/\sqrt{S} > x_0$. The broadening can only affect a relatively small fraction of the W and Z bosons with $|y| \gtrsim \ln[M_V/(\sqrt{S}x_0)] \sim 2$, and it has negligible influence on most of the Tevatron observables. The feasibility of discovering q_T broadening at the Tevatron depends on the available detector acceptance in the forward-rapidity regions. The rapidity coverage of the D0 and CDF detectors is reviewed in the appendix. Our estimates suggest that

---

[4]The rapidity distributions and other observables inclusive in q_T are insensitive to the q_T broadening in our model, due to the Gaussian form of the broadening exponential assumed in Eq. (23).
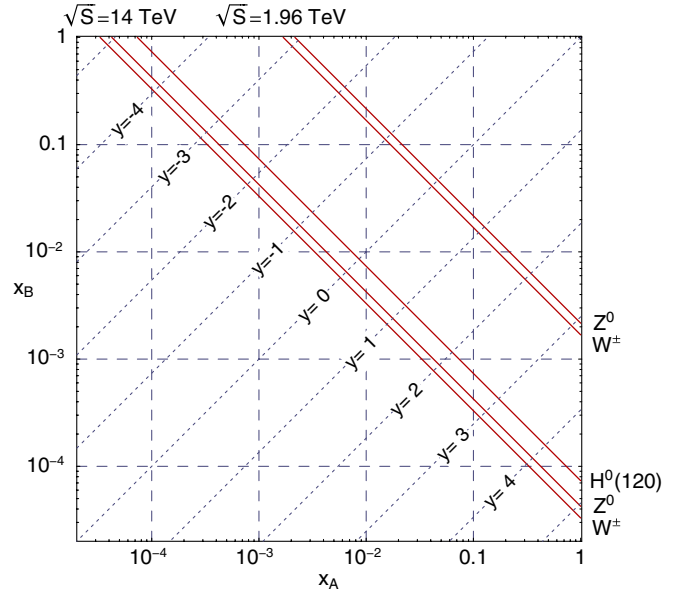

FIG. 1 (color online). Parton momentum fractions x_A and x_B accessible in W, Z, and Higgs boson production (for $M_H = 120$ GeV) in the Tevatron Run-2 ($\sqrt{S} = 1.96$ TeV) and at the LHC ($\sqrt{S} = 14$ TeV). The accessible ranges of x_A and x_B are shown by the solid lines. The contours of the constant rapidity y are shown by the inclined dotted lines.

verification of q_T broadening at the Tevatron is viable in the near future.

At the LHC ($\sqrt{S} = 14$ TeV), at least one momentum fraction x_A or x_B is of order, or less than, x_0 in all W and Z boson events. Consequently the broadening is important at all rapidities. The magnitude of the broadening at the LHC generally differs between Z, W^+, and W^- bosons, as a result of their different masses and rapidity distributions. The smaller mass of W bosons is conducive to the broadening. 70% of W^+ bosons are produced in $u\bar{d}$ annihilation, enhanced at $|y| > 1.5$ by contributions from valence u quarks. Most of W^- and Z bosons are produced in scattering of valence d quarks and/or sea quarks, which tends to put more events in the central-rapidity region. Consequently the fraction of forward-rapidity events is larger in W^+ boson production than in W^- or Z boson production, and, of the three boson species, the W^+ bosons are the most sensitive to the broadening. The decay of $W^{\pm}$ bosons mixes contributions from different ranges of $|y|$, reducing the differences between q_T broadening effects in the lepton-level observables.

The Higgs bosons with the mass in the experimentally allowed range ($M_H > 115$ GeV) are produced via gluon fusion at somewhat larger momentum fractions, such as $M_H/\sqrt{S} \sim 0.0086$ for $M_H = 120$ GeV. Their rapidity distribution in Fig. 2(c) is narrower than in the W and Z boson cases due to the suppression of the forward-rapidity regions by the decreasing gluon density $g(x)$ at $x \rightarrow 1$. Consequently the broadening is reduced in the Higgs boson signal, but may be important in the background processes.
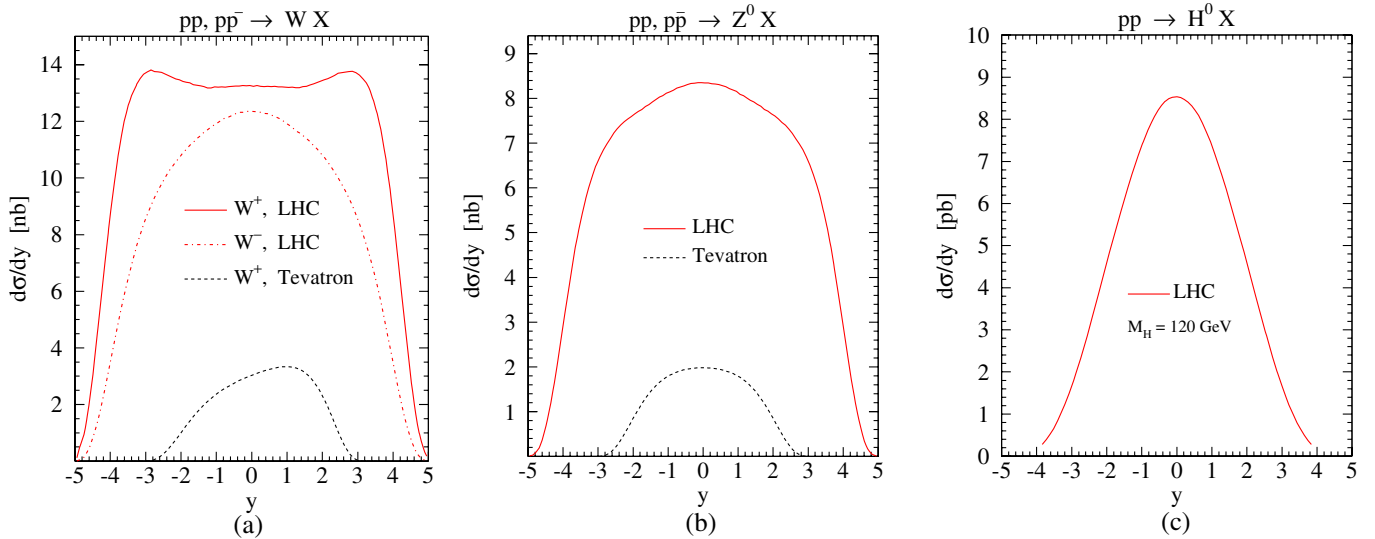
FIG. 2 (color online).   Rapidity distributions $d\sigma/dy$ for (a) $W^\pm$ boson production at the Tevatron and LHC; (b) Z^0 boson production at the Tevatron and LHC; and (c) Higgs boson production at the LHC.

Next, we present the quantitative results for the individual scattering processes.

B. W and Z boson production in the Tevatron Run-2

1. Z boson production

The broadening may be most easily observed in the dilepton channel in Z boson production in the Tevatron Run-2. The strategy here is to exclude contributions from the central-rapidity Z bosons, which are almost insensitive to the broadening. If no distinction between the central and forward Z bosons is made (as, e.g., in the Run-1 analysis), the small-x broadening contributes at the level of the other uncertainties in the resummed form factor. Figure 3(a) shows the Z boson distribution $d\sigma/dq_T$, integrated over the Z boson rapidity y without selection cuts on the decay leptons. The cross section with the broadening term (dashed line) essentially coincides with the cross section without such a term (solid line). Both cross sections are dominated by contributions from $x \sim M_Z/\sqrt{S} \sim 0.046 \gg x_0$, where the broadening function $\rho(x)$ is negligible.

In contrast, the small-x broadening visibly modifies $d\sigma/dq_T$ at forward rapidities, where one of the initial-state partons carries a smaller momentum fraction than in the central region. Figure 3(b) shows the cross section $d\sigma/dq_T$ for Z bosons satisfying $|y| > 2$. The peak of the curve with $\rho(x) \neq 0$ is lower and shifted toward higher q_T. Figure 3(c) displays the cross sections with the acceptance cuts $y_{e^\pm} > 2$, $p_{Te^\pm} > 20$ GeV or $y_{e^\pm} < -2$, $p_{Te^\pm} > 20$ GeV simultaneously imposed on both decay leptons. The cuts exclude contributions with $|y| < 2$ and retain a fairly large cross section (≈ 3.4 pb), most of which falls within the acceptance region (extending up to $|y_e| \approx 3$ in the D0
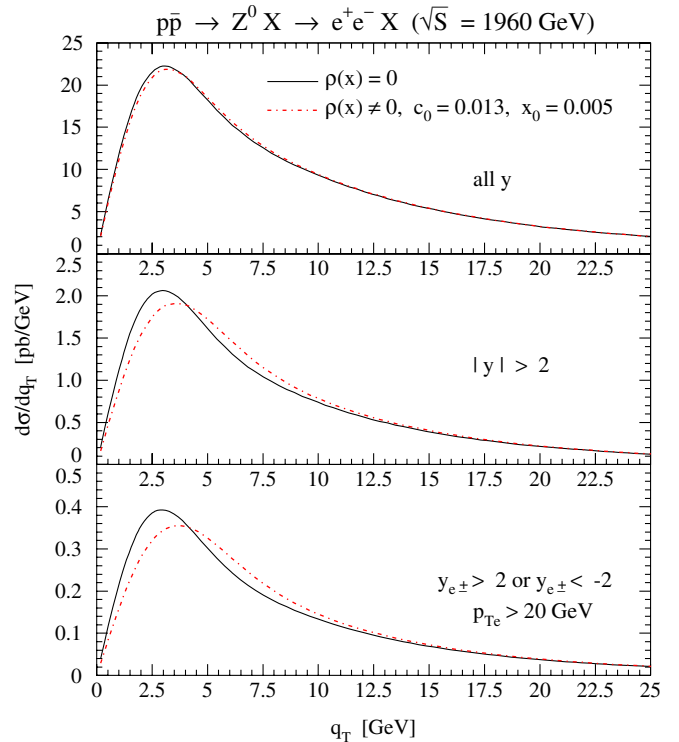

FIG. 3 (color online).   Transverse momentum distributions of Z bosons in the Tevatron Run-2: (a) integrated over the full range of Z boson rapidity y; (b) for events with a large Z boson rapidity, $|y| > 2$; (c) for events with both decay electrons registered in the forward ($y_{e^+} > 2$, $y_{e^-} > 2$, and $p_{Te^\pm} > 20$ GeV) or backward ($y_{e^+} < -2$, $y_{e^-} < -2$, and $p_{Te^\pm} > 20$ GeV) detector regions. The solid curve is the standard CSS cross section, calculated using the BLNY parametrization [9] of the nonperturbative Sudakov factor. The dashed curve includes additional terms responsible for the q_T broadening in the small-x region, as in Eq. (23).

detector). The Run-2 can probably discriminate between the curves in Fig. 3(c) given the improved acceptance and increased luminosity of the upgraded Tevatron collider.

To estimate sensitivity of the Tevatron Z boson production to uncertainties in the model for q_T broadening, we vary the control parameter x_0 [cf. Equation (22)] within the limits compatible with the analyzed SIDIS z-flow data. The parameter x_0 determines the upper boundary of the x range in which the broadening effects are important. As was observed in Ref. [26], the q_T-broadening was required in most of the range $x \in [10^{-4}, 10^{-2}]$ in SIDIS in order to obtain a good fit to $d\Sigma_z/dq_T$ from Refs. [27,28]. Given this observation, $x_0 = 0.005$ assumed in Fig. 3 is a conservative estimate of the upper boundary of the x region impacted by the broadening at HERA. Values of x_0 as high as 10^{-2} are compatible with the HERA data, while $x_0 \sim 10^{-3}$ or smaller would lead to a poor fit to the HERA data in the range $x \in [x_0, 10^{-2}]$.

If x_0 lies in the range 10^{-3}-10^{-2}, the broadening remains observable at the Tevatron. Figure 4 shows the cross sections for $x_0 = \{0.002, 0.005, 0.008\}$, compared to the standard BLNY result. Although the broadening is reduced for $x_0 = 0.002$, it may still be discernible in a high-statistics data sample. On the other hand, the broadening can be also enhanced for $x_0 > 0.005$, as demonstrated by the curve for $x_0 = 0.008$. The magnitude of the broadening for a given x_0 is affected by the parameter c_0, which is anticorrelated with the power of x in the phenomenological factor $e^{-c_0 b^2/x^p}$ found in the SIDIS fit. Adjustments in c_0 can be compensated in some range by varying p and without deteriorating the overall quality of the SIDIS fit. For example, the central value $c_0 = 0.013$ was obtained for $p = 1$ in the best fit [26] to both sets of the z-flow data [27,28]. The best fit to the earlier of the two H1 data sets [27] was obtained in Ref. [25] for $e^{-S_{NP}^z} = \exp[-4.58 + 0.58/\sqrt{x}]$, i.e., reduction in the negative power of x from 1 to 0.5 was partly compensated by the increase of c_0 from 0.013 to 0.58. The magnitude of the broadening at the Tevatron for the superseded $1/\sqrt{x}$ parametrization is even

larger than that shown in Fig. 4. Correlated uncertainties in the parameters of the SIDIS fit (and possibly a combined SIDIS/Drell-Yan fit) can be constrained in a future dedicated study, especially after improved SIDIS data from HERA-2 become available.

2. W boson production

In the absence of leptonic cuts, W boson production is slightly more sensitive to the small-x broadening as compared to Z boson production because of the smaller mass and wider rapidity distribution of the W boson. The relevant q_T distributions are displayed in Fig. 5. As in the case of the Z boson, the broadening is essentially negligible in the absence of selection cuts on y or leptonic momenta [cf. Figure 5(a)]. In the forward region $|y| > 2$ [Fig. 5(b)], the broadening term shifts the peak of $d\sigma/dq_T$ significantly. The change $\delta q_T \approx 750$ MeV in the position of the peak is larger than the analogous change $\delta q_T \approx 500$ MeV in the Z boson cross section.

Integration over the unobserved neutrino's rapidity in the $e\nu$ decay channel mixes contributions from different
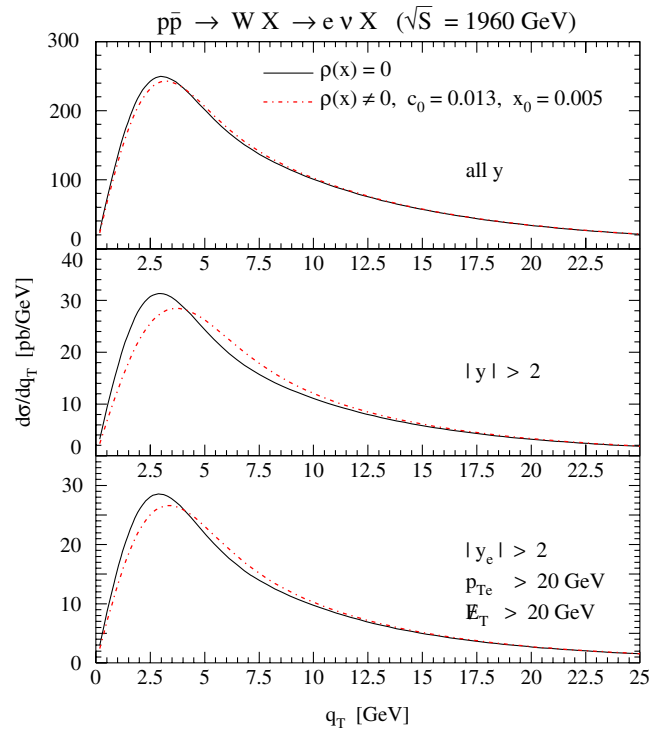
FIG. 5 (color online). Transverse momentum distributions for a combined sample of W^+ and W^- bosons in the Tevatron Run-2; (a) integrated over the full range of W boson rapidities; (b) integrated over the forward boson rapidities $|y| > 2$; (c) integrated with the selection cuts $|y_e| > 2$, $p_{Te} > 20$ GeV, $\not{E}_T > 20$ GeV. The solid curve is the standard CSS cross section, calculated using the BLNY parametrization [9] of the nonperturbative Sudakov factor. The dashed curve includes additional terms responsible for the q_T broadening in the small-x region, as in Eq. (23).
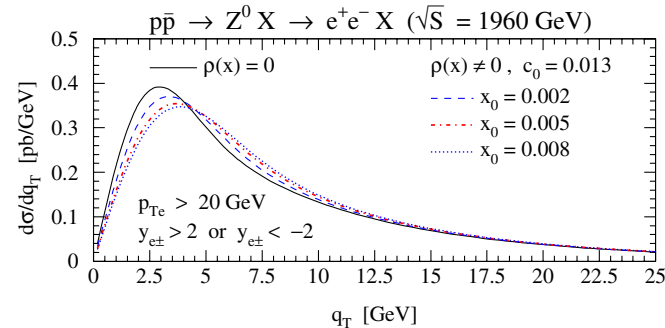
FIG. 4 (color online). Same as Fig. 3(c), for the BLNY parametrization (solid line), and various choices of the parameter x_0 in Eq. (22): $x_0 = 0.002$ (dashed line), 0.005 (dot-dashed line), and 0.008 (dotted line).

rapidities of W bosons, thus enhancing the broadening at central electron rapidities and reducing the broadening at forward electron rapidities. The strongest effect occurs when only forward electrons are selected. Figure 5(c) shows the cross sections $d\sigma/dq_T$ with constraints imposed on the momentum of the electron ($|y_e| > 2$, $p_{Te} > 20$ GeV) and missing transverse energy associated with the neutrino ($\not{E}_T > 20$ GeV). Although visible, the difference between the solid and dashed curves in Fig. 5(c) is less pronounced than in the W boson-level distribution in Fig. 5(b) or in the Z-boson lepton-level distribution in Fig. 3(c). This is because some events in the sample with a forward electron rapidity and arbitrary neutrino rapidity are due to the decay of central-rapidity W bosons, which are not affected by the broadening. In contrast, events with two forward high-p_T electrons in Z boson production are always due to the decay of forward-boosted Z bosons, and they are more sensitive to the broadening effects.

Despite its modest magnitude, the forward q_T broadening may affect the precision measurement of the W boson mass M_W in the Tevatron Run-2. The current goal of CDF and D0 experiments is to measure M_W with the accuracy of $30-40$ MeV per experiment. The W boson mass is commonly extracted from the distribution with respect to the leptonic transverse mass [63], defined by

$$M_T^{e\nu} \equiv \sqrt{(|\mathbf{p}_{Te}| + |\mathbf{p}_{T\nu}|)^2 - (\mathbf{p}_{Te} + \mathbf{p}_{T\nu})^2} \qquad (39)$$

in terms of the transverse momentum $\mathbf{p}_{Te}$ of the electron and transverse momentum $\mathbf{p}_{T\nu}$ of the neutrino. In the experiment, the neutrino's transverse momentum is equated to the missing transverse energy, $|\mathbf{p}_{T\nu}| = \not{E}_T$. The determination of M_W from the shape of the kinematical (Jacobian) peak in $d\sigma/dM_T^{e\nu}$ is scarcely sensitive to the boson's transverse momentum q_T.[5] We have verified that the impact of the broadening on $d\sigma/dM_T^{e\nu}$ is negligible. However, reconstruction of $\not{E}_T$ introduces a sizable uncertainty in the determination of M_W by the $M_T^{e\nu}$ method. An alternative method is to extract M_W from the distribution $d\sigma/dp_{Te}$. This method does not suffer from the complications associated with the reconstruction of $\not{E}_T$, but, as a trade-off, it is directly sensitive to the transverse momentum q_T of the W bosons. In practice, the final uncertainties on M_W from the transverse mass and transverse momentum methods are comparable. As we will now show, the q_T broadening can substantially affect M_W determined from the transverse momentum of electrons in the forward calorimeter.

The distribution $d\sigma/dp_{Te}$ is shown in Fig. 6. Its Jacobian peak is located at $p_{Te} \sim M_W/2 \approx 40$ GeV. To better visualize percent-level changes in $d\sigma/dp_{Te}$ associ-

---

[5]More precisely, a variation δq_T in the typical transverse momentum results in an error of order $\delta M_T^{e\nu}/M_T^{e\nu} \sim \delta q_T^2/M_W^2 \ll 1$ in the typical transverse mass.
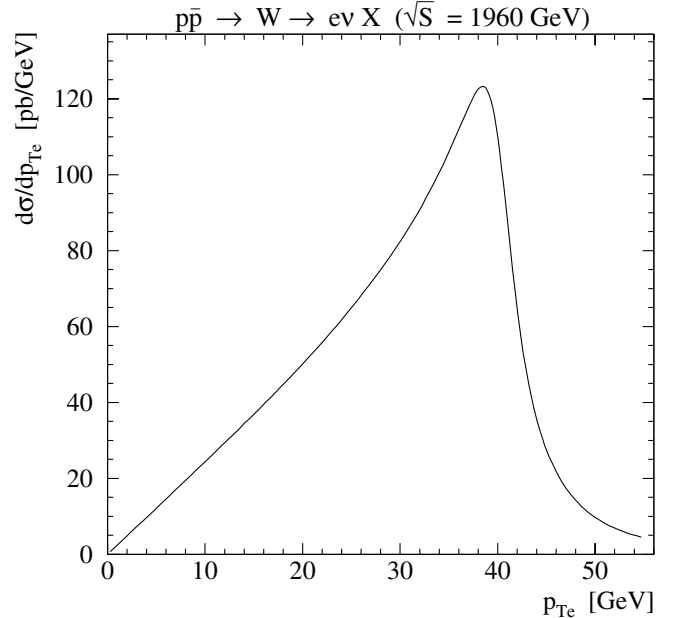

FIG. 6. Transverse momentum distribution $d\sigma/dp_{Te}$ of the electrons from the decay of W bosons in the Tevatron Run-2. CTEQ6M parton densities [62] and BLNY nonperturbative Sudakov factor [9] were used.

ated with the broadening, we plot in Fig. 7 the fractional difference $(d\sigma^{\text{mod}}/dp_{Te})/(d\sigma^{\text{std}}/dp_{Te}) - 1$ of the "modified" (mod) and "standard" (std) theory cross sections. The standard cross sections are obtained by taking $\rho(x) = 0$ and some reference value of M_W, which we choose to be equal to 80.423 GeV. The modified cross sections are obtained by taking either $\rho(x) \neq 0$ (dotted curve) or a slightly varied W boson mass, $M_W + 50$ MeV (dashed curve), and $M_W - 50$ MeV (dot-dashed curve). The impact of q_T broadening on the measurement of M_W can be judged by comparing the fractional differences due to the inclusion of the broadening term $\rho(x) \neq 0$ and explicit variation of M_W by ± 50 MeV for $\rho(x) = 0$.

A small increase of M_W results in a positive shift of the Jacobian peak, which reduces the cross section at $p_{Te} < M_W/2$ and increases the cross section at $p_{Te} > M_W/2$. A decrease in M_W shifts the Jacobian peak in the opposite direction. The broadening of $d\sigma/dq_T$ shifts the Jacobian peak in the positive direction. At $|y_e| < 1$ or in the rapidity-inclusive sample, the broadening can be mistaken for an increase of M_W by $10-20$ MeV, as well as uncertainties in the parton distributions and/or nonperturbative Sudakov factor [cf. Figure 7(a)]. At $|y_e| > 1$, the small-x broadening exceeds the other theoretical uncertainties and is comparable with a variation of M_W by more than 50 MeV [cf. Figure 7(b)]. It remains observable even if the electron's energy is smeared due to the finite resolution of the detector. The experimental fractional resolution $\delta E/E$ near the Jacobian peak is typically less than 3% [64,65]. We have estimated the energy smearing by convolving $d\sigma/dp_{Te}$
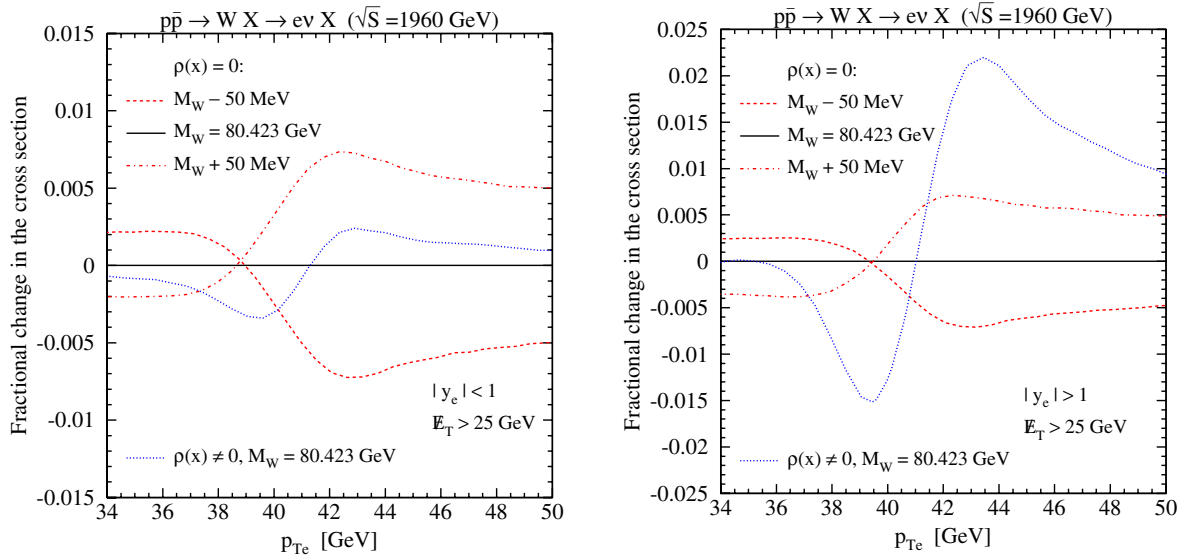
FIG. 7 (color online). The fractional difference in the distribution $d\sigma/dp_{Te}$: (a) for the central-rapidity sample of electrons ($|y_e| < 1$), and (b) for the forward-rapidity sample of electrons ($|y_e| > 1$). The shown curves are explained in the main text.

with the Gaussian functions of the width corresponding to $\delta E/E$ between 1% and 5%. In all cases, the variation in the smeared $d\sigma/dp_{Te}$ due to the broadening has exceeded variations due to the shift of M_W by ± 50 MeV.

C. Electroweak boson production at the Large Hadron Collider

1. W and Z bosons

At the LHC, the small-x broadening may be observed in W and Z boson production at all rapidities. Very forward vector bosons probe x down to $\sim 3 \cdot 10^{-5}$, while the SIDIS data constrains the b-dependent parton distributions at x above $\sim 10^{-4}$. To stay in the kinematic region probed by the SIDIS data, we restrict our analysis to the events in the central-rapidity region, which we define by requiring the rapidities of the decay electrons to be less than 2.5.
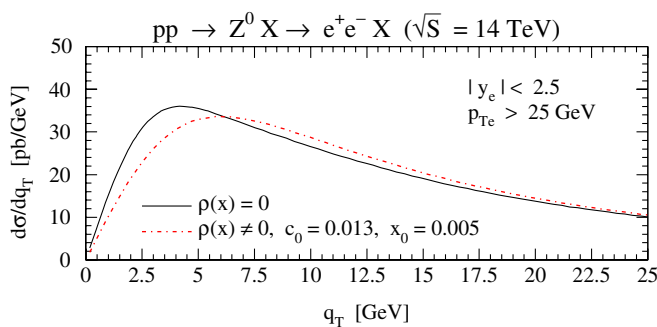
Figure 8 demonstrates q_T distributions of centrally produced Z bosons, selected by imposing the cuts $|y_e| < 2.5$ and $p_{Te} > 25$ GeV on both decay electrons. The distribution with $\rho(x) \neq 0$ is shifted toward higher q_T. The broadening shift exceeds typical uncertainties in S_{NP}: a similar shift would result from the increase of $S_{NP}(b, M_Z; b_*)$ from $\approx 3.2b^2$ in the BLNY parametrization to $\approx 8b^2$. The q_T shift is even larger in production of W bosons [cf. Figure 9], which we evaluate by requiring $|y_e| < 2.5$, $p_{Te} > 25$ GeV, and $\not{E}_T > 25$ GeV. The smaller mass M_W and less restrictive leptonic cuts result in smaller typical x
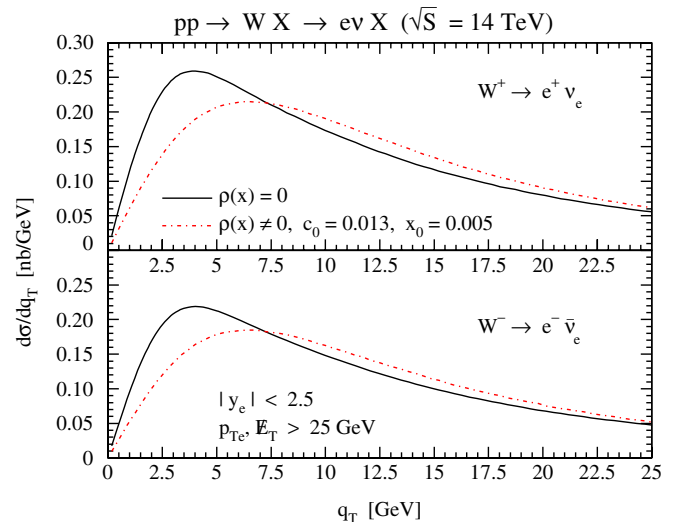

FIG. 9 (color online). Transverse momentum distributions of (a) W^+ bosons and (b) W^- bosons at the Large Hadron Collider. The decay leptons are required to satisfy $|y_e| < 2.5$, $p_{Te} > 25$ GeV, $\not{E}_T > 25$ GeV.

FIG. 8 (color online). Transverse momentum distributions of Z bosons at the Large Hadron Collider. The events are selected by requiring $|y_e| < 2.5$ and $p_{Te} > 25$ GeV for both decay electrons.
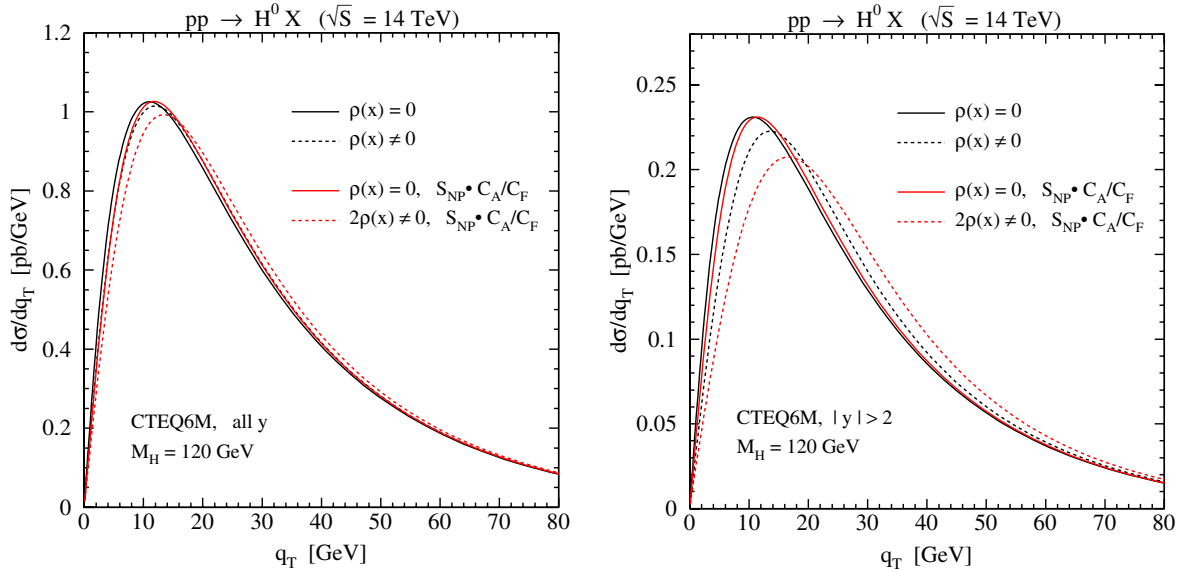
FIG. 10 (color online). The transverse momentum distribution $d\sigma/dq_T$ for on-shell Higgs bosons at the Large Hadron Collider: (a) integrated over the full range of boson rapidities; (b) integrated over the forward region $|y| > 2$. The meaning of the curves is explained in the text.

probed by the W bosons, hence, in stronger broadening. The shift is slightly larger in W^+ boson production [cf. Figure 9(a)] as compared to W^- boson production [cf. Figure 9(b)] because of the flatter y distribution for W^+ bosons [cf. Figure 2(a)]. The shown q_T broadening propagates into the leptonic transverse mass and transverse momentum distributions. Both $M_T^{e\nu}$ and $p_{T\ell}$ methods for the measurement of M_W may be affected in this case, in contrast to the Tevatron, where the $M_T^{e\nu}$ method is not susceptible to the broadening.

2. Higgs boson

The small-x broadening is less spectacular, but visible, in the production of light Higgs bosons via the effective ggH vertex. Standard model Higgs bosons with mass below about 140 GeV can be distinguished above the continuum background by their decay into a pair of highly energetic photons. The photon pairs produced from the Higgs boson decay have a larger typical q_T than the photon pairs produced from the dominant background processes $q\bar{q} \to \gamma\gamma$ and $gg \to \gamma\gamma$.[6] For this reason, selection of photon pairs with q_T above 20–30 GeV can improve the statistical significance of the Higgs boson signal.

The harder q_T spectrum of the gg-dominated Higgs boson signal results from the larger leading-logarithm

coefficient $\mathcal{A}^{(1)}$ in the perturbative Sudakov factor (equal to $C_A = 3$ in gg channels and $C_F = 4/3 = (4/9)C_A$ in $q\bar{q}$ channels). The Higgs boson q_T distribution peaks at $q_T \sim 10$-20 GeV, as compared to $q_T \sim 5$-10 GeV in $q\bar{q}$-dominated Z boson distribution. A harder q_T spectrum weakens the impact of the nonperturbative Sudakov function [61] and q_T broadening. The broadening in the rapidity-inclusive Higgs boson cross section is further reduced because of the heavier Higgs boson mass and suppression of the forward-rapidity regions, as displayed in Fig. 2(c). The nonperturbative and q_T broadening terms in gg-initiated processes are not constrained yet by the data. In the following, we evaluate the uncertainty in the Higgs boson q_T distribution by computing the resummed cross sections for several plausible choices of $\rho(x)$ and $S_{NP}(b, Q; b_*)$.

Figure 10(a) shows q_T distributions for on-shell Higgs bosons with a mass $M_H = 120$ GeV and arbitrary rapidity. We first compare the cross sections for $\rho(x) = 0$ and $\rho(x) \neq 0$ (thick lines), with the same functions $\rho(x)$ and $S_{NP}(b, Q; b_*)$ as in Z boson production. The difference between the two curves is minimal. The value of $\mathcal{A}^{(1)}$ reflects the dominant color flow in the scattering. The bigger $\mathcal{A}^{(1)}$ in Higgs boson production suggests that the Q-dependent part (and possibly other terms) in S_{NP} may be multiplied by a larger color factor than in the Drell-Yan process. To estimate this effect, we multiply S_{NP} by $C_A/C_F = 9/4$. The resulting cross section (thin solid line) is close to the other cross sections.

The $\ln(1/x)$ terms in Higgs boson production may be enhanced as well, due to the direct coupling of the Higgs

---

[6]We refer to each hard subprocess according to its Born-level contribution, but the resummed cross sections include the relevant higher-order corrections to the Born-level diagram. For instance, the resummed cross section for $q\bar{q} \to \gamma\gamma$ also includes the contributions from $q\bar{q} \to \gamma\gamma g$, $qg \to \gamma\gamma q$, etc.

bosons to gluon ladders. However, the broadening would have to be quite large to affect q_T of 20 GeV or more, i.e., near the location of the selection cuts on q_T of the photon pair. For example, increasing the function $\rho(x)$ by a factor of 2 as compared to the Z boson case would lead to a distribution shown by the thin dashed line, which remains close to the other cross sections at q_T above 20 GeV. The broadening is enhanced in the sample with $|y| > 2$, which constitutes about 20% of the total cross section [Fig. 10(b)]. In this figure, the differences between the curves are more substantial at all q_T. The theoretical uncertainties seen in Fig. 10(b) will have to be reduced to reliably predict Higgs boson production at forward rapidities.

The small-x broadening will be also present in the main background channels, $q\bar{q} \to \gamma\gamma$ and $gg \to \gamma\gamma$. Application of the CSS formalism in these channels was discussed in Refs. [66–68]. The dominant background process, $q\bar{q} \to \gamma\gamma$, has the same structure of the resummed cross section as $q\bar{q} \to Z^0$. In analogy to Z boson production, the broadening effect in $q\bar{q} \to \gamma\gamma$ is expected to be stronger than in $gg \to H^0$ or $gg \to \gamma\gamma$, so that the selection cut on q_T of the $\gamma\gamma$ pair may have to be revised. Additional measurements will be needed to constrain the small-x behavior in the gg channel, e.g., by examining Υ production [69,70] or $\gamma\gamma$ production away from the Higgs signal region. As the mass of the photon pair decreases, the subprocess $gg \to \gamma\gamma$ becomes increasingly important, contributing about 40% of the total cross section at $Q = 80$ GeV at the LHC [71]. By comparing q_T distributions in $pp \to \gamma\gamma$ and $pp \to Z$ in the same region of Q, one may be able to separate the $q\bar{q}$ and gg components of the resummed cross section and learn about the x dependence in the gg channel.

IV. CONCLUSION

In this paper, we analyze consequences of possible nontrivial rapidity dependence in transverse momentum distributions of massive electroweak bosons at the Tevatron and LHC. A specific mechanism considered here assumes enhancement of radiative corrections in the impact-parameter-dependent parton distributions at $x \lesssim 10^{-2}$. This enhancement can explain the semi-inclusive DIS data from HERA, and it leads to wider transverse momentum distributions in the forward-rapidity regions at hadron colliders. A measurement of the rapidity dependence of q_T distributions will test for the presence of such effects and verify universality of b-dependent parton distributions, which was used in this paper to relate the SIDIS and Drell-Yan cross sections.

Because of the two-scale nature of the transverse momentum resummation, large radiative corrections (such as nonresummed $\ln(1/x)$ terms) may affect the q_T distribution even when they leave no discernible trace in the inclusive cross sections depending on one hard scale Q. The Collins-

Soper-Sterman resummed form factor depends on the impact parameter b, which specifies the factorization scale $\sim 1/b$ in the b-dependent parton distributions. This scale changes from zero to infinity when b is integrated over the whole range in the Fourier-Bessel transform to obtain the resummed q_T distribution. When $1/b$ is much smaller than Q, the series $\alpha_s^m(1/b)\ln^n(1/x)$ in the CSS formula diverge at a larger value of x than the series $\alpha_s^m(Q)\ln^n(1/x)$ in the inclusive cross sections. For this reason, the transition to the small-x dynamics may occur at larger x in q_T distributions than in one-scale observables.

For a realistic choice of parameters, the rapidity-dependent q_T broadening may be discovered via the analysis of forward-produced Z bosons at the Tevatron Run-2. The broadening could be also searched for in the production of Drell-Yan pairs with a mass of a few GeV in fixed-target and collider experiments. Because of the different masses and shapes of the rapidity distributions for $W^{\pm}$, Z^0, and Higgs bosons, the magnitude of the broadening depends on the type and charge of the boson produced, and selection cuts imposed on the decay products. In the Tevatron Run-2, the resulting change may shift the measured W boson mass in the p_{T_e} method by 10–20 MeV in the central region ($|y_e| < 1$) and more than 50 MeV in the forward region ($|y_e| > 1$).

At the LHC, the most striking consequence is a harder q_T distribution for W bosons displayed in Fig. 9. The predicted effect may easily exceed the other uncertainties in the resummed cross section, resulting in important implications for the measurement of the W boson mass from both transverse mass and transverse momentum distributions. The selection requirements imposed on the Higgs boson candidates in the $\gamma\gamma$ decay channel may have to be reconsidered to account for the nonuniform broadening in the signal and background processes. More generally, the broadening may bring about a revision of the earlier predictions that have neglected the correlation between the transverse momentum and rapidity in Drell-Yan-like processes.

APPENDIX: DETECTOR ACCEPTANCES AT THE TEVATRON AND LHC

In this appendix, we review the angular coverage of the hadronic detectors and discuss feasibility of the observation of q_T broadening at the Tevatron and LHC.

In the Tevatron Run-2, adequate detector acceptance at large pseudorapidities $\eta = -\log(\tan(\theta/2)$ is crucial for the observation of q_T broadening in Z boson production at $y \approx |\eta| \gtrsim 2$. Z bosons can be identified by registering two high-p_T electrons in the electromagnetic calorimeter, with simultaneous positive identification of at least one electron by the tracking system. In the D0 detector, the silicon tracking system extends out to $|\eta| \sim 3$ [72–74], which provides an excellent opportunity for collecting a clean sample of forward-boosted Z bosons in events with two registered forward electrons.

At CDF [75], the unambiguous selection of the forward-boosted Z bosons is not possible due to the absence of tracking in the forward region. The CDF detector can efficiently track charged electrons in the main drift chamber at $|\eta| < 1$ and in the silicon system at $|\eta| < 2$. Low efficiency tracking can be done up to $|\eta| \sim 2.6$ by taking advantage of the longitudinally displaced collision vertex in a fraction of events. Energy deposits from the electrons can be registered in the plug calorimeter up to $|\eta| \sim 3.6$. To increase sensitivity in the forward region, CDF could concentrate on events with one central ($|\eta| < 2$) and one forward ($|\eta| > 2$) electron. Despite contamination by central Z bosons, this sample may reveal the small-x broadening once enough events are accumulated in the next years of Run-2.

The q_T broadening in Z boson production can be also detected in muon decays. However, the coverage of the Tevatron muon systems ($|\eta| < 1.5$ at CDF and $|\eta| < 2$ at D0) may be insufficient in the kinematic region affected by the broadening.

Excellent opportunities to probe the x dependence of q_T distributions will become available at the LHC. Because of the larger center-of-mass energy, the q_T broadening may affect W and Z boson production at all rapidities. In the ATLAS experiment, the tracking in the inner detector extends up to $|\eta| \sim 2.5$. The central and forward electromagnetic calorimeters cover $|\eta| < 4.9$, and the muon chambers cover $|\eta| < 2.7$ [76]. In the CMS detector, the inner tracking system will register the high-p_T charged particles in the range $|\eta| < 2.5$. The electromagnetic calorimeter extends up to $|\eta| = 3$ [77]. Eventually, the TOTEM experiment will extend charged particle tracking and triggering capabilities of the CMS experiment into the range $3 < |\eta| < 6.8$ [78].

[1] G. Degrassi, S. Heinemeyer, W. Hollik, P. Slavich, and G. Weiglein, Eur. Phys. J. C **28**, 133 (2003).
[2] R. K. Ellis and S. Veseli, Nucl. Phys. **B511**, 649 (1998).
[3] A. Guffanti and G. E. Smye, J. High Energy Phys. 10 (2000) 025.
[4] A. Kulesza and W. J. Stirling, Eur. Phys. J. C **20**, 349 (2001).
[5] A. Kulesza, G. Sterman, and W. Vogelsang, Phys. Rev. D **66**, 014011 (2002).
[6] X. Ji, J.-P. Ma, and F. Yuan, Phys. Rev. D **71**, 034005 (2005).
[7] X. Ji, J.-P. Ma, and F. Yuan, Phys. Lett. B **597**, 299 (2004).
[8] J. C. Collins, D. E. Soper, and G. Sterman, Nucl. Phys. **B250**, 199 (1985).
[9] F. Landry, R. Brock, P. M. Nadolsky, and C.-P. Yuan, Phys. Rev. D **67**, 073016 (2003).
[10] S. Berge, P. Nadolsky, F. Olness, and C.-P. Yuan, hep-ph/0401128.
[11] M. Dobbs *et al.*, hep-ph/0403100.
[12] Y. L. Dokshitzer, Sov. Phys. JETP **46**, 641 (1977).
[13] V. N. Gribov and L. N. Lipatov, Yad. Fiz. **15**, 781 (1972) [Sov. J. Nucl. Phys. **15**, 438 (1972)].
[14] V. N. Gribov and L. N. Lipatov, Yad. Fiz. **15**, 1218 (1972) [Sov. J. Nucl. Phys. **15**, 675 (1972)].
[15] G. Altarelli and G. Parisi, Nucl. Phys. **B126**, 298 (1977).
[16] I. I. Balitsky and L. N. Lipatov, Sov. J. Nucl. Phys. **28**, 822 (1978).
[17] E. A. Kuraev, L. N. Lipatov, and V. S. Fadin, Sov. Phys. JETP **44**, 443 (1976).
[18] E. A. Kuraev, L. N. Lipatov, and V. S. Fadin, Sov. Phys. JETP **45**, 199 (1977).
[19] M. Ciafaloni, Nucl. Phys. **B296**, 49 (1988).
[20] S. Catani, F. Fiorani, and G. Marchesini, Phys. Lett. B **234**, 339 (1990).
[21] S. Catani, F. Fiorani, and G. Marchesini, Nucl. Phys. **B336**, 18 (1990).
[22] G. Marchesini, Nucl. Phys. **B445**, 49 (1995).
[23] J. C. Collins, Nucl. Phys. **B396**, 161 (1993).
[24] R. Meng, F. I. Olness, and D. E. Soper, Phys. Rev. D **54**, 1919 (1996).
[25] P. Nadolsky, D. R. Stump, and C.-P. Yuan, Phys. Rev. D **61**, 014003 (2000); **64**, 059903(E) (2001).
[26] P. M. Nadolsky, D. R. Stump, and C.-P. Yuan, Phys. Rev. D **64**, 114011 (2001).
[27] S. Aid *et al.* (H1 Collaboration), Phys. Lett. B **356**, 118 (1995).
[28] C. Adloff *et al.* (H1 Collaboration), Eur. Phys. J. C **12**, 595 (2000).

[29] B. A. Kniehl, G. Kramer, and M. Maniatis, Nucl. Phys. **B711**, 345 (2005).

[30] P. Aurenche, R. Basu, M. Fontannaz, and R. M. Godbole, Eur. Phys. J. C **34**, 277 (2004).

[31] M. Fontannaz, Eur. Phys. J. C **38**, 297 (2004).

[32] A. Daleo, D. de Florian, and R. Sassot, Phys. Rev. D **71**, 034013 (2005).

[33] M. Ciafaloni, D. Colferai, G. P. Salam, and A. M. Stasto, Phys. Lett. B **587**, 87 (2004).

[34] J. C. Collins and A. Metz, Phys. Rev. Lett. **93**, 252001 (2004).

[35] J. R. Ellis, M. K. Gaillard, and D. V. Nanopoulos, Nucl. Phys. **B106**, 292 (1976).

[36] M. A. Shifman, A. I. Vainshtein, M. B. Voloshin, and V. I. Zakharov, Yad. Fiz. **30**, 1368 (1979) [Sov. J. Nucl. Phys. **30**, 711 (1979)].

[37] S. Dawson, Nucl. Phys. **B359**, 283 (1991).

[38] A. Djouadi, M. Spira, and P. M. Zerwas, Phys. Lett. B **264**, 440 (1991).

[39] J. Kodaira and L. Trentadue, Phys. Lett. B **112**, 66 (1982).

[40] C. T. H. Davies and W. J. Stirling, Nucl. Phys. **B244**, 337 (1984).

[41] S. Catani, E. D'Emilio, and L. Trentadue, Phys. Lett. B **211**, 335 (1988).

[42] R. P. Kauffman, Phys. Rev. D **44**, 1415 (1991).

[43] C.-P. Yuan, Phys. Lett. B **283**, 395 (1992).

[44] D. de Florian and M. Grazzini, Phys. Rev. Lett. **85**, 4678 (2000).

[45] S. Catani, D. de Florian, and M. Grazzini, Nucl. Phys. **B596**, 299 (2001).

[46] J. C. Collins and D. E. Soper, Nucl. Phys. **B194**, 445 (1982).

[47] J. C. Collins and D. E. Soper, Nucl. Phys. **B197**, 446 (1982).

[48] C. T. H. Davies, B. R. Webber, and W. J. Stirling, Nucl. Phys. **B256**, 413 (1985).

[49] G. A. Ladinsky and C. P. Yuan, Phys. Rev. D **50**, R4239 (1994).

[50] R. K. Ellis, D. A. Ross, and S. Veseli, Nucl. Phys. **B503**, 309 (1997).

[51] F. Landry, R. Brock, G. Ladinsky, and C.-P. Yuan, Phys. Rev. D **63**, 013004 (2001).

[52] F. J. Landry, Ph.D. thesis, Michigan State University, 2001, UMI-30-09135-mc (microfiche).

[53] J. Qiu and X. Zhang, Phys. Rev. D **63**, 114011 (2001).

[54] G. P. Korchemsky and G. Sterman, Nucl. Phys. **B555**, 335 (1999).

[55] S. Tafat, J. High Energy Phys. 05 (2001) 004.

[56] R. D. Peccei and R. Ruckl, Phys. Lett. B **84**, 95 (1979).

[57] R. D. Peccei and R. Ruckl, Nucl. Phys. **B162**, 125 (1980).

[58] M. Dechantsreiter, F. Halzen, and D. M. Scott, Z. Phys. C **8**, 85 (1981).

[59] J. C. Collins and D. E. Soper, Nucl. Phys. **B193**, 381 (1981); **B213**, 545(E) (1983).

[60] C. Balazs and C.-P. Yuan, Phys. Rev. D **56**, 5558 (1997).

[61] C. Balazs and C.-P. Yuan, Phys. Lett. B **478**, 192 (2000).

[62] J. Pumplin et al., J. High Energy Phys. 07 (2002) 012.

[63] J. Smith, W. L. van Neerven, and J. A. M. Vermaseren, Phys. Rev. Lett. **50**, 1738 (1983).

[64] T. Affolder et al. (CDF Collaboration), Phys. Rev. D **64**, 052001 (2001).

[65] V. M. Abazov et al. (D0 Collaboration), Phys. Rev. D **66**, 012001 (2002).

[66] C. Balazs, E. L. Berger, S. Mrenna, and C.-P. Yuan, Phys. Rev. D **57**, 6934 (1998).

[67] C. Balazs, P. Nadolsky, C. Schmidt, and C.-P. Yuan, Phys. Lett. B **489**, 157 (2000).

[68] P. M. Nadolsky and C. R. Schmidt, Phys. Lett. B **558**, 63 (2003).

[69] A. Kulesza and W. J. Stirling, J. High Energy Phys. 12 (2003) 056.

[70] E. L. Berger, J.-W. Qiu, and Y.-L. Wang, Phys. Rev. D **71**, 034007 (2005).

[71] Z. Bern, L. J. Dixon, and C. Schmidt, Phys. Rev. D **66**, 074018 (2002).

[72] S. Abachi et al. (D0 Collaboration), Nucl. Instrum. Methods Phys. Res., Sect. A **338**, 185 (1994).

[73] S. Hagopian, in Proceedings of 7th International Conference on Advanced Technology and Particle Physics, Italy, 2001 (unpublished).

[74] J. Ellison (D0 Collaboration), hep-ex/0101048.

[75] F. Abe et al. (CDF Collaboration), Nucl. Instrum. Methods Phys. Res., Sect. A **271**, 387 (1988).

[76] The ATLAS Collaboration, *ATLAS: detector and physics performance*, Technical Design Report No. CERN-LHCC-99-14, Vol. 1, 1999 (unpublished); The ATLAS Collaboration, *ATLAS: detector and physics performance*, Technical Design Report No. CERN-LHCC-99-15, Vol. 2, 1999 (unpublished).

[77] The CMS Collaboration, *The electromagnetic calorimeter project*, Technical Design Report No. CERN-LHCC-97-33, 1997 (unpublished).

[78] V. Berardi et al., TOTEM: Technical Design Report No. CERN-LHCC-2004-002, 2004 (unpublished).